Chiral tunneling in single-layer graphene with Rashba spin-orbit coupling: Spin currents

Y. Avishai[1,2,3,*] and Y. B. Band ®[1,4]

[1]*Department of Physics, Ben-Gurion University of the Negev, Beer-Sheva 8410501, Israel*
[2]*New York University and the NYU-ECNU Institute of Physics at NYU Shanghai,*
3663 Zhongshan Road North, Shanghai, 200062, China
[3]*Yukawa Institute for Theoretical Physics, Kyoto 606-8502, Japan*
[4]*Department of Chemistry, Department of Electro-Optics, and The Ilse Katz Center for Nano-Science,*
Ben-Gurion University of the Negev, Beer-Sheva 8410501, Israel

We study forward scattering of two-dimensional massless Dirac electrons at Fermi energy $\varepsilon > 0$ in single-layer graphene (SLG) through a one-dimensional rectangular barrier of height u_0 in the presence of uniform Rashba spin-orbit coupling (of strength λ). The role of the Klein paradox in graphene spintronics is thereby exposed. It is shown that (1) for $\varepsilon - 2\lambda < u_0 < \varepsilon + 2\lambda$, there is partial Klein tunneling, the transmission coefficient $T(\lambda) < 1$, and quite remarkably, $T(\lambda \geqslant 0.1 \text{ meV}) \approx 0$ when the scattering energy equals the barrier height $\varepsilon = u_0$ [whereas $T(\lambda = 0) = 2$]. (2) Spin density and spin-current density are remarkably different than in bulk SLG. They are sensitive to λ and u_0. (3) Spin current densities are space dependent, implying the occurrence of nonzero spin torque density. Such a system may serve as a graphene-based spintronic device without the use of an external magnetic field or magnetic materials.

I. INTRODUCTION

Shortly after the discovery of graphene [1], numerous novel physical phenomena were revealed in its electronic properties [2,3]. One of these, the occurrence of chiral tunneling and the Klein paradox [4] in single-layer graphene (SLG), was reported in a seminal paper [5]. This work was further expanded in Refs. [6–8]. It was shown that, due to chirality near a Dirac point, electrons execute unimpeded transmission for energies below the potential barrier. This phenomenon is related to the absence of backscattering for electron-impurity scattering in carbon nanotubes [9]. Several additional extensions have been reported in Refs. [10–12]. In parallel, investigation of the role of electron spin in graphene led to the emergence of a field: graphene spintronics [13–56].

Here, we study Klein tunneling of two-dimensional (2D) massless Dirac electrons at Fermi energy $\varepsilon > 0$ in SLG, through a one-dimensional (1D) barrier of height u_0 in the presence of uniform Rashba spin-orbit coupling (RSOC) of strength λ [57]. The motivation is to elucidate the effect of the Klein paradox on observables such as spin density, spin current density, and spin torque [58]. The calculated spin observables have properties that are remarkably different from those predicted in bulk SLG [48] (i.e., in the absence of a 1D potential so that the Klein paradox does not play a role). Symmetry relations are broken (see below), and the spin current is space dependent so that there is a finite spin torque. Most importantly, the response of the spin densities to the RSOC strength is substantial even for small RSOC coupling (the

strength of Rashba splitting caused by a strong electric field in SLG is reported in Ref. [45] to be a fraction of an meV). Hence, we hope that our paper will motivate the fabrication of graphene-based spintronic devices that do not rely on the use of an external magnetic field or magnetic materials.

In addition to the study of spin-related observables, we also expose the occurrence of *partial Klein tunneling*, which causes an intriguing behavior of the transmission coefficient T. Explicitly, the pertinent scattering problem involves two scattering channels. In the narrow region $\varepsilon - 2\lambda < u_0 < \varepsilon + 2\lambda$ (for $\lambda > 1$ meV), only one scattering channel is open, and $T < 1$. Moreover, for scattering energy equal to the barrier height $\varepsilon = u_0$, one channel just closes while the second channel just opens, and $T \approx 0$ (recall that $T = 2$ for $\lambda = 0$).

In the sections below, we present the formalism used (Sec. II), explain the choice of parameters (Sec. III), analyze the properties of the transmission (Sec. IV), derive expressions and present results for spin density and spin current density (Sec. V), and conclude with a short summary (Sec. VI). Some technical steps and additional figures are relegated to the Appendix.

II. FORMALISM

Consider massless 2D Dirac electrons in SLG (lying in the x-y plane) that are scattered from a 1D rectangular potential barrier of $u(x) = u_0 \Theta(x)\Theta(d - x)$ and subject to a uniform electric field $\mathbf{E} = E_0\hat{\mathbf{z}}$. Our treatment is carried out within the continuum formulation near one of the Dirac points, say $\mathbf{K}'$, and focuses on forward scattering $k_y = 0$ (rendering the problem 1D). Recall that, in addition to the isospin $\boldsymbol{\tau}$ encoding the two-lattice structure of graphene, there is now a *real spin* $\boldsymbol{\sigma}$.

*yshai@bgu.ac.il

The pertinent Hamiltonian (in units where the kinetic energy parameter $\hbar v_F = 1$) is

$$h(-i\partial_x, \lambda) = [-i\partial_x + \lambda(\hat{\mathbf{z}} \times \boldsymbol{\sigma})_x]\tau_x + \lambda(\hat{\mathbf{z}} \times \boldsymbol{\sigma})_y\tau_y + u(x)$$

$$\equiv h_0(-i\partial_x, \lambda) + u(x), \quad (1)$$

which is a 4×4 matrix first-order differential operator in $\boldsymbol{\sigma} \otimes \boldsymbol{\tau}$ space acting on the four component wave function $\psi(x)$ subject to scattering boundary conditions. The wave function $\psi(x)$ is expressible as a combination of plane-wave vectors $\exp(\pm ik_x x)v(\pm k_x)$ for $x \notin [0, d]$), and $\exp(\pm iq_x x)w(\pm q_x)$ for $x \in [0, d]$. Here, k_x, q_x, ε, u_0, and λ are expressed in $(\text{nm})^{-1}$, and d is expressed in nm. However, in presenting our numerical results below, energies ε, u_0, and RSOC strength λ are presented in meV, $[1 \, (\text{nm})^{-1} = 659.107 \text{ meV}]$. The four component vectors $v(\pm k_x)$ and $w(\pm q_x)$ have unit current density $v^{\dagger}\hat{j}_x v = w^{\dagger}\hat{j}_x w = 1$, where $\hat{j}_x = \frac{1}{A}I_{2 \times 2} \otimes \tau_x$ is the current operator, and A is an area unit. They satisfy the equations

$$h_0(\pm k_x, \lambda)v(\pm k_x) = \varepsilon v(\pm k_x),$$

$$h(\pm q_x, \lambda)w(\pm q_x) = \varepsilon w(\pm q_x). \quad (2)$$

Because RSOC acts in all space (not only in the barrier region), the vectors $v(\pm k_x)$ cannot be chosen as spin eigenfunctions since spin is not conserved. The equations in Eq. (2) are not eigenvalue equations. Rather, they are implicit equations for the wave numbers $k_x(\varepsilon)$ and $q_x(\varepsilon)$, which depend on the fixed scattering energy as well as for $u[\pm k_x(\varepsilon)]$ and $w[\pm q_x(\varepsilon)]$. For $\varepsilon > 0$, there are two wave numbers in each region that solve these implicit equations, $\pm k_{xn}(\varepsilon)$ for $x \notin [0, d]$, and $\pm q_{xn}(\varepsilon)$ for $x \in [0, d]$ ($n = 1, 2$). The solution of Eq. (2) yields (see Appendix)

$$k_{xn}^2 = [\varepsilon + (-1)^{n+1}\lambda]^2 - \lambda^2,$$

$$q_{xn}^2 = [\varepsilon + (-1)^{n+1}\lambda - u_0]^2 - \lambda^2. \quad (3)$$

The wave function corresponding to an incoming wave in channel n ($n = 1, 2$) in the three regions is

$$\psi_n(x) = \begin{cases} \underbrace{|k_{xn}\rangle + r_{n1}|\bar{k}_{x1}\rangle + r_{n2}|\bar{k}_{x2}\rangle}_{x<0} \\ \underbrace{a_{n1}^+|q_{x1}\rangle + a_{n2}^+|q_{x2}\rangle + a_{n1}^-|\bar{q}_{x1}\rangle + a_{n2}^-|\bar{q}_{x2}\rangle}_{0<x<d}, \\ \underbrace{t_{n1}|k_{x1}\rangle + t_{n2}|k_{x2}\rangle}_{x>d} \end{cases} \quad (4)$$

where $|k_{xn}\rangle \equiv \exp(ik_{xn}x)v_n(k_{xn})$, $|\bar{k}_{xn}\rangle \equiv |-k_{xn}\rangle$, $|q_{xn}\rangle \equiv \exp(iq_{xn}x)w_n(q_{xn})$, and $|\bar{q}_{xn}\rangle \equiv |-q_{xn}\rangle$.

The matching conditions at $x = 0$ and $x = d$ yield the transmission and reflection amplitude matrices $t = \begin{pmatrix} t_{11}t_{12} \\ t_{21}t_{22} \end{pmatrix}$ and $r = \begin{pmatrix} r_{11}r_{12} \\ r_{21}r_{22} \end{pmatrix}$ together with the eight coefficients $\{a_{nm}^{\pm}\}$, ($n, m = 1, 2$). The wave functions $\psi_n(x)$ with scattering boundary conditions are therefore determined everywhere. The solution obeys unitarity and current conservation:

$$T + R = \text{Tr}[t^{\dagger}t] + \text{Tr}[r^{\dagger}r] = 2,$$

$$\frac{d}{dx}j(x) \equiv \frac{d}{dx}\sum_{n=1}^{2}\psi_n^{\dagger}(x)\hat{j}_x\psi_n(x) = 0. \quad (5)$$

Here, T and R are the transmission and reflection coefficients, and $\hat{j}_x = I_2 \otimes \tau_x$ is the current operator defined after Eq. (2).
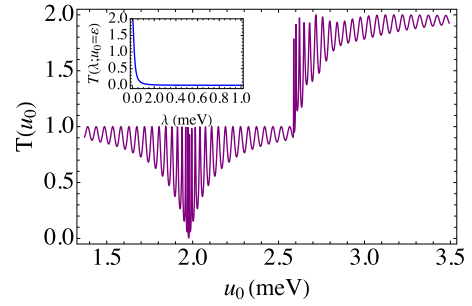

FIG. 1. Partial Klein tunneling ($T < 1$) and full Klein tunneling ($1 < T < 2$) through a barrier of small height u_0 occurs when $|u_0 - \varepsilon| < 2\lambda$ (partial) and $u_0 > \varepsilon + 2\lambda$ (full). For $\varepsilon = 1.977$ meV, $\lambda = 0.30314$ meV, and $d = 60$ nm, T is plotted vs u_0 in the range $\varepsilon - 2\lambda < u_0 < 3.5$ meV. A remarkable feature of RSOC is that, for $u_0 \approx \varepsilon$ (where channel 1 is about to close and channel 2 is about to open), T nearly vanishes except for $\lambda \to 0$ where, as shown in the inset, it sharply rises to 2 [see Eq. (6)].

The numerical choice of parameters is dictated by experiments. In Ref. [45], it is shown that, for a field $E_R = 2$ V/nm, λ is of the order of a fraction of 1 meV. Here, we let $0 < \lambda \leqslant 0.659$ meV and vary the barrier height in the range $0 < u_0 < 200$. The barrier width d is taken at 200 nm (except for Fig. 1, where $d = 60$ nm). Concerning the choice of ε, it is expected that the interesting physics occurs for ε close to λ. The reason is that the RSOC partially lifts the spin degeneracy, and at the Dirac point, the energy splitting is of the order of λ. The role of electron spin is relevant when the scattering energy is close to the two split levels (see Fig. 8(b) in Ref. [34]).

III. TRANSMISSION

For $k_y = 0$, the two channels are uncoupled, and the transmission coefficient is obtained analytically:

$$T(u_0; \varepsilon, \lambda) = \sum_{n=1}^{2} \frac{q_{xn}^2}{(u_0 - \varepsilon)[(u_0 - \varepsilon) + 4\lambda] - \lambda^2 \sin^2(q_{xn}d)}. \quad (6)$$

A necessary condition for the occurrence of Klein tunneling is $k_n^2 > 0, n = 1, 2 \Rightarrow \varepsilon > 2\lambda > 0$. *Full Klein tunneling* occurs if $q_n^2 > 0, n = 1, 2$, i.e., $u_0 > \varepsilon + 2\lambda$. If $(q_1 q_2)^2 < 0$, i.e., $\varepsilon > u_0 > 2\lambda > 0$ (where $q_{x1}^2 > 0, q_{x2}^2 < 0$), or $\varepsilon + 2\lambda > u_0 > \varepsilon - 2\lambda > 0$ (where $q_{x1}^2 < 0, q_{x2}^2 > 0$), we have *partial Klein tunneling*. If $q_{xn}^2 < 0$, the corresponding denominator in Eq. (6) is very large so that the contribution of this term to the transmission is minuscule because $-\sin^2(q_{xn}d) = \sinh^2(|q_{xn}|d) \gg 1$, and channel n is virtually closed. Thus, Klein tunneling is still manifest even if only one channel is open, but then $T \leqslant 1$. Inspecting $T(u_0; \varepsilon, \lambda)$ as a function of u_0 in Fig. 1 shows that, when the scattering energy equals the barrier height ($\varepsilon = u_0$, where channel 1 is about to close and channel 2 is about to open), $T(u_0; \varepsilon = u_0, \lambda) \approx 0$. Recall from Eq. (6) that, for $\lambda = 0$, the transmission at the forward direction is unimpeded $T(u_0; \varepsilon, \lambda = 0) = 2$ (identically). However, the inset in Fig. 1 shows that this happens for very small λ. Note that, in the corresponding 1D Schrödinger problem for $\varepsilon = u_0$, $T = \frac{4}{4+(kd)^2}$, where $k = \sqrt{\frac{2m\varepsilon}{\hbar^2}}$. Therefore, an experimental measurement of
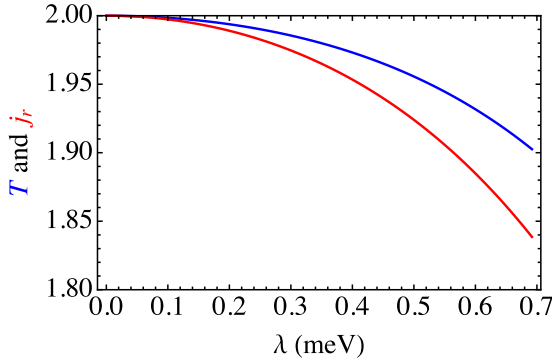
FIG. 2. Transmission T (blue) and current j_x (red) for the p-n-p junction vs λ for $u_0 = 195$ meV, $d = 200$ nm, $\varepsilon = 6.65$ meV, and $k_y = 0$ [recall that, for $\lambda = 0$, $T(k_y = 0) = 2$ identically].

transmission for $\lambda \neq 0$ should be an excellent probe of the strength of RSOC in SLG.

We now consider the transmission coefficient T and the (matter) current $j(x)$ as a function of potential barrier height parameter $u_0 > \varepsilon + 2\lambda$ and the RSOC strength parameter λ. Figure 2 shows the transmission and current vs λ for fixed u_0, and Fig. 8(a) in the Appendix shows the transmission and current vs u_0 for fixed λ. The main conclusion from these figures is that, in the presence of RSOC, the transmission coefficient is no longer unimpeded. Rather, for fixed u_0 and for experimentally relevant interval $0 < \lambda < 0.65$ meV, the transmission smoothly decreases as in Fig. 1. For fixed λ, considered as a function of the barrier height u_0, it shows a pattern of oscillations below the unitarity upper limit $T = 2$, as shown in Fig. 8(a) in the Appendix. It is of course not surprising that the current and the transmission coefficient are highly correlated. Note that the current is space independent [see before Eq. (2)].

IV. SPIN DENSITY

Spin density (and spin current density) operators $\{\mathcal{O}\}$ are representable as 4×4 matrices in $\boldsymbol{\sigma} \otimes \boldsymbol{\tau}$ space. Spin observables are obtained as $O(x) = \psi^\dagger(x) \mathcal{O} \psi(x)$ (this is not an expectation value; spin observables may depend on x). The spin density operators $\hat{\mathbf{S}}$ and the spin density observables $\mathbf{S}(x)$ are given by

$$\hat{\mathbf{S}} = \tfrac{1}{2}\hbar \boldsymbol{\sigma} \otimes \mathbf{I}_2, \quad \mathbf{S}(x) = \frac{1}{4} \sum_{n=1}^{2} \psi_n^\dagger(x) \hat{\mathbf{S}} \psi_n(x), \quad (7)$$

where $\psi_n(x)$ is defined in Eq. (4). The unit of spin density used here is $S_0 = \hbar/A$. As expected, $S_x = S_z = 0$ because the polarization is proportional to $\mathbf{k} \times \mathbf{E} \parallel \hat{\mathbf{y}}$, and here, $k_y = 0$. Figure 3 shows the spin density S_y as a function of λ (spin densities are space independent). The polarization increases rapidly for $\lambda > 0.20$ meV. Figure 8(b) in the Appendix plots S_y vs u_0 and shows a rich oscillatory pattern that decreases near the lower limit $u_0 = \varepsilon + 2\lambda$, below which one channel is closed (see discussion of Fig. 1). Both figures substantiate the role of λ and u_0 as useful parameters to control the degree of polarization.
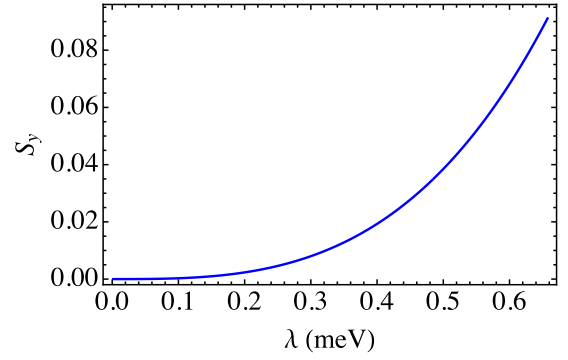

FIG. 3. Spin density S_y versus λ for $u_0 = 192$ meV, $d = 200$ nm, $\varepsilon = 2.60$ meV, and $k_y = 0$.

V. SPIN CURRENT DENSITY OPERATORS AND OBSERVABLES

The (tensor) spin current density operator $\mathbb{J}$ and the observed components of the spin current density $J_{ij}(x)$ are defined as

$$\hat{\mathbb{J}} = \frac{1}{2}\{\hat{\mathbf{S}}, \hat{\mathbf{V}}\}, \quad \Rightarrow \quad \hat{\mathbb{J}}_{i,j} = \hat{S}_i \hat{V}_j + \hat{V}_j \hat{S}_i,$$

$$J_{ij}(x) = \frac{1}{2} \sum_{n=1}^{2} \psi_n^\dagger(x) \hat{\mathbb{J}}_{ij} \psi_n(x), \quad (8)$$

where $\hat{\mathbf{S}}$ is the spin density operator defined in Eq. (7), and $\hat{\mathbf{V}} = \mathbf{I}_2 \otimes \boldsymbol{\tau}$ is the velocity operator $[= \hat{j}_x$ defined before Eq. (2)]. In Eq. (8), $i = 1, 2, 3 = x, y, z$ specifies the polarization direction, and $j = 1, 2 = x, y$ the direction of propagation. The unit of spin current density is $J_0 = S_0 v_F = \gamma/A = 659.107$ meV/nm.

The spin current density was calculated in bulk SLG in Ref. [48]; it was found that (1) $J_{xx} = J_{yy} = J_{zx} = J_{zy} = 0$, (2) $J_{xy} = -J_{yx}$, and (3) the spin currents are independent of space (see Eq. (5) in Ref. [48]). Below, we show that (1) in the presence of a 1D potential (where there is no rotational symmetry around the z axis), the symmetry relation $J_{xy} = -J_{yx}$ that is valid in bulk SLG [48] is broken. (2) Although the value of λ used in our calculations is much smaller than that used in Ref. [48], the size of spin current densities of both systems is the same. (3) The spin current densities are not uniform, and the continuity equation includes a spin torque density term [58] (see below). Figure 4 shows $J_{xy}(d)$ and $J_{yx}(d)$ as a function of λ. Note the nearly linear increase of, e.g., $J_{xy}(d)$ with λ. No symmetry exists between J_{xy} and J_{yx}. Figures 9(a) and 9(b) in the Appendix show the spin current densities $J_{xy}(0)$ (red curve) and $J_{yx}(0)$ (blue curve) just at the left wall of the barrier, for the p-n-p junction as a function of λ and u_0 respectively. The size of the spin current density $J_{xy}(0)$ (electrons polarized along x and propagated along y) for $\lambda \approx 0.659$ meV is indeed large (as compared with J_{xy} in bulk SLG calculated for $\lambda \approx 45$ meV).

To stress the role of the Klein paradox in the present system, we compare our results with those obtained in bulk SLG (where there is no Klein paradox). In eq. (7) of Ref. [48], the authors found that, in bulk SLG, $J_{yx} = J_0 \frac{\eta^2 + \cos 2\phi}{1 + \eta^2}$, where $\eta =$
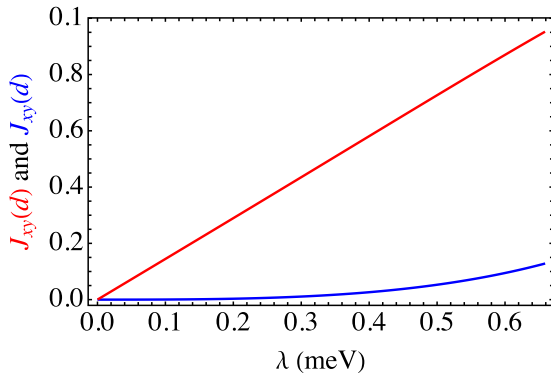
FIG. 4. Spin current densities J_{yx} and J_{xy} (in units of J_0) vs λ at the right wall of the barrier ($x = d$) vs λ for $u_0 = 192$ meV, $d = 200$ nm, and $\varepsilon = 2.60$ meV. Note that the symmetry condition $J_{xy} = -J_{yx}$ valid in bulk single-layer graphene (SLG) [48] is broken by the one-dimensional (1D) potential barrier.

$\frac{\varepsilon}{\sqrt{k_x^2 + k_y^2}}$ is of the order of unity, and $\phi = \arctan k_y/k_x$. Thus, for $k_y = 0$, this implies $J_{yx} = -J_{xy} \approx J_0$. As shown in Figs. 4–6, in the presence of 1D potential barrier, the spin current density can reach similar values. However, in Ref. [48], the value of λ is about 200 times higher than the one we have used. As shown in Ref. [45], such high values of λ are not achievable in SLG. It is possible to have higher values of RSOC if the SLG is in contact with metals such as Au or Pb. However, upon passing a current through the metallic substrate, the electrons will flow through the metal and not through the SLG, so at the Fermi level, the electronic states are metallic.

Spin current densities vs u_0 are shown in Fig. 5. Recalling the behavior of $S_y(u_0)$ shown in Fig. 8(b)

in the Appendix and of $J_{xy}(u_0)$ and $J_{yx}(u_0)$ in Fig. 5, it is clear that the spin density and the spin current density are significantly correlated.

Consider now the space dependence of the spin current densities $J_{xy}(x)$ and $J_{yx}(x)$ (recall that the spin density **S** is space independent). They are plotted in Fig. 6 to the left of the barrier (the reflected region), where the wave numbers k_{xn} [defined in the first row of Eq. (3)], are small (since ε and λ are small). This space dependence results in nonzero divergence, and the corresponding continuity equation requires
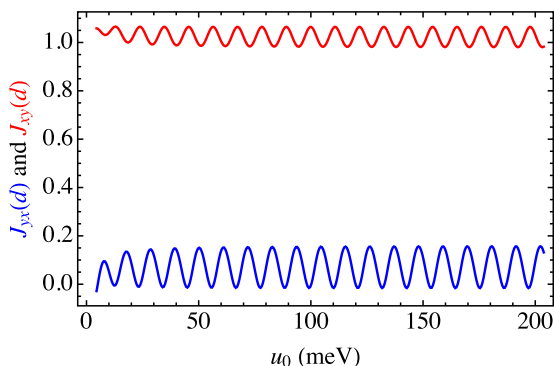

FIG. 5. Spin current densities $J_{xy}(d)$, $J_{yx}(d)$ on the right wall of the barrier vs λ for $\varepsilon + 2\lambda < u_0 < 200$ meV, $d = 200$ nm, $\varepsilon = 2.60$ meV, $\lambda = 0.695$ meV, and $k_y = 0$.
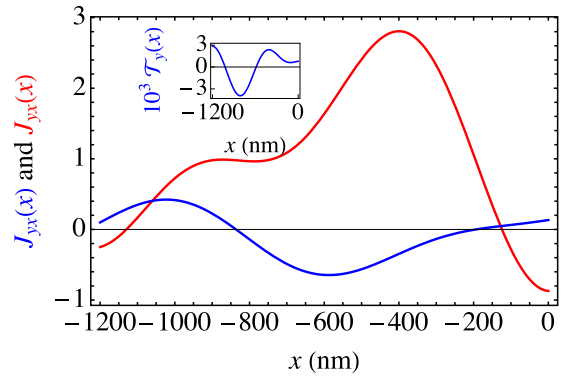

FIG. 6. Space dependence of the spin current densities $J_{xy}(x)$ and $J_{yx}(x)$ (in units of J_0) for $-1200 < x < 0$ nm (region to the left of the barrier, where the wave is reflected) for $\lambda = 0.695$ meV, $\varepsilon = 2.60$ meV, and $u_0 = 198.2$ meV. Oscillations due to the linear combination of plane waves continues to $x \to -\infty$. The inset shows the spin torque density $\mathcal{T}_y(x)$ in units of $J_0/$nm.

the inclusion of finite spin torque density $\mathcal{T}_i$, ($i = x, y, z$) [58]. Following the discussion in Sec. 3 of Appendix, there are two relevant vector fields $\mathbf{J}_1(x) = [0, J_{xy}(x)]$ and $\mathbf{J}_2(x) = [J_{yx}(x), 0]$ that satisfy continuity equations $\nabla \cdot \mathbf{J}_i = \mathcal{T}_i$. Therefore, in our case, the only nonzero spin torque density is $\mathcal{T}_2(x) = dJ_{yx}(x)/dx$. As shown in Fig. 6, in the region $x < 0$, $J_{yx}(x)$ is smooth, and the spin torque density derived from it is well defined (and measurable).

VI. SUMMARY AND CONCLUSION

The Klein paradox in SLG occurs at the Fermi energy ε when an electron tunnels through a 1D potential barrier of height u_0 (which can be experimentally controlled by a gate voltage) in the region $u_0 > \varepsilon > 0$. When, in addition, a uniform perpendicular electric field $\mathbf{E} = E_0\hat{\mathbf{z}}$ is applied, the role of electron spin enters due to RSOC. Here, we elucidate the physics when the Klein paradox and RSOC are combined to expose interesting facets of graphene spintronics within a time-reversal invariant formalism. The fact that u_0 and λ can be easily experimentally controlled makes our analysis readily verifiable.

Our main results can be summarized in terms of the figures. (1) Transmission coefficient T: Due to partial Klein tunneling, $0 < T < 1$ for $|u_0 - \varepsilon| < 2\lambda$, and $T \approx 0$ for $\varepsilon = u_0$ and $\lambda > 0.2$ meV (Fig. 1). For $u_0 > \varepsilon + 2\lambda$, the transmission decreases smoothly as a function of λ (Fig. 2). Recall that $T = 2$ for $\lambda = 0$ and $k_y = 0$. (2) Spin density: $S_x = S_z = 0$, and as shown in Fig. 3, the space-independent spin density $S_y(\lambda)$ increases rapidly with λ. (3) Spin current densities $J_{ij}(x)$: As shown in Figs. 4–6: The symmetry $J_{xy} = -J_{yx}$ in bulk SLG is broken, J_{xy} increases linearly with λ, and both $J_{xy}(x)$ and $J_{yx}(x)$ are space dependent, the continuity equation for $J_{yx}(x)$ includes a nonzero spin torque density [58]. Clearly, in the present system (as compared with bulk SLG), spin density and spin current density have a much richer behavior.

Complimenting the developments in spintronics [59,60], this paper is partially motivated by the quest for constructing spintronic devices without the use of an external magnetic field or magnetic materials [61–63]. Specifically for graphene,
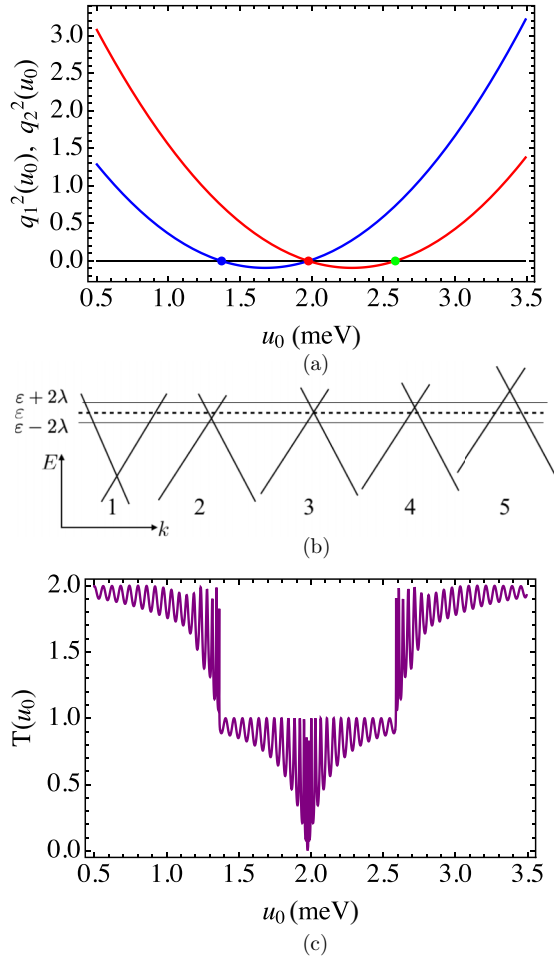
(a)

(b)

(c)

FIG. 7. Various configurations related to Klein transmission through a barrier of height u_0, in the presence of Rashba spin-orbit coupling (RSOC) of strength λ, when $|u_0 - \varepsilon| < 2\lambda$. Here, we take $\varepsilon = 1.977$ meV, $\lambda = 0.30314$ meV, and barrier width $d = 60$ nm. (a) Squared wave numbers q_{xn}^2 defined in Eq. (3) (blue for $n = 1$ and red for $n = 2$). The blue, green, and red points mark $u_0 = (\varepsilon - 2\lambda, \varepsilon, \varepsilon + 2\lambda)$. Negative q_{xn}^2 implies that channel n is closed (does not contribute to the transmission). (b) Dirac cones for various values of u_0 (schematic), Fermi energy ε and spin-order splitting $\varepsilon \pm 2\lambda$ (magnified): In panels 1–5, $u_0 = 0$, $\varepsilon - \lambda$, ε, $\varepsilon + \lambda$, and $u_0 > \varepsilon + 2\lambda$. (c) The total transmission is plotted vs u_0 for $\varepsilon - 2\lambda < u_0 < 3.5$ (meV). A remarkable feature of RSOC is that, for $u_0 \approx \varepsilon$ [red point in (a) where one channel is about to open and the other is about to close], the transmission nearly vanishes except very near λ, as shown in the inset of Fig. 1, where it sharply rises to 2 [see Eq. (7)].

it shows the vanishing of the transmission at energy $\varepsilon = u_0$, the linear dependence of spin current density $J_{xy}(d)$ on λ, and the occurrence of spin torque density, thereby advancing this goal.
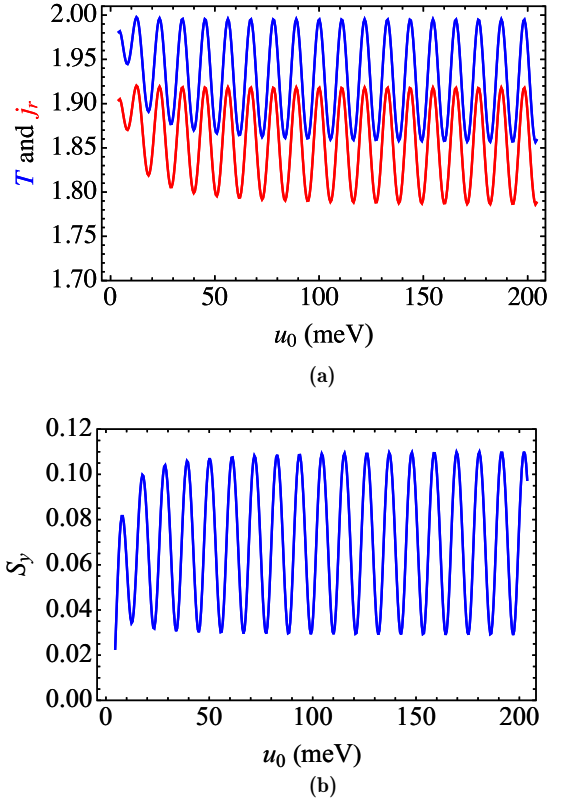
ACKNOWLEDGMENTS

(a)

(b)

FIG. 8. (a) Transmission T (blue) and current j_x (red) for the p-n-p junction vs u_0 in the range $\varepsilon + 2\lambda < u_0 < 200$ meV for $\lambda = 0.695$ meV. Other parameters as in Fig. 1. (b) Spin density S_y vs $\varepsilon + 2\lambda < u_0 < 200$ meV for $\lambda = 0.695$ meV and $k_y = 0$. Other parameters are as in Fig. 3. Note that $S_y(x)$ is independent of x throughout the sample.

APPENDIX

Here, we briefly expand on several points discussed in the main text. Recall that the pertinent system consists of electron scattering in SLG at Fermi energy ε that undergoes Klein tunneling through a 1D rectangular barrier of height u_0, width ℓ, and subject to a RSOC of strength λ. The main topics clarified below include (1) derivation of Eqs. (2) and (3); (2) additional details on the occurrence of partial Klein tunneling in the region $\varepsilon - 2\lambda \leqslant u_0 \leqslant \varepsilon + 2\lambda$ and its dramatic effect on the transmission in this region; (3) additional figures showing the spin current density as a function of the barrier height u_0 and the RSOC strength λ; (4) discussion of the space dependence of spin current density, the pertinent continuity relation, and its relation to the spin torque density [58].

1. Equations (2) and (3)

The precise form of $h_0(k_x, k_y, \lambda)$ in Eq.(2), in the general case $k_y \neq 0$, is

$$h_0(k_x, k_y, \lambda) = \begin{pmatrix} 0 & k_x - ik_y & 0 & 0 \\ k_x + ik_y & 0 & 2i\lambda & 0 \\ 0 & -2i\lambda & 0 & k_x - ik_y \\ 0 & 0 & k_x + ik_y & 0 \end{pmatrix}.$$

(A1)

Its two positive eigenvalues are

$$\varepsilon_{1,2} = \mu(k_x, k_y, \lambda) \mp \lambda, \qquad (A2)$$

where

$$\mu(k_x, k_y, \lambda) \equiv \sqrt{k_x^2 + k_y^2 + \lambda^2}. \qquad (A3)$$

The corresponding eigenvectors are

$$v_{1,2}(k_x, k_y) = \frac{1}{2}\sqrt{1 \pm \frac{\lambda}{\mu(k_x, k_y, \lambda)}} \begin{Bmatrix} \mp i k_x + k_y \\ i[\lambda \mp \mu(k_x, k_y, \lambda)] \\ \mp \lambda + \mu(k_x, k_y, \lambda) \\ k_x + i k_y \end{Bmatrix}. \qquad (A4)$$

For $k_y = 0$ (forward propagation) and fixed scattering energy ε, this means that the energies in Eq. (A2) are both equal $\varepsilon_1 = \varepsilon_2 = \varepsilon$. Solving for k_x in each equation yields the two wave numbers $\{k_{xn}(\varepsilon)\}$ ($n = 1, 2$) specified in Eq. (3). These wave numbers, when inserted into the vectors $v_{1,2}(k_x)$ defined in Eq. (A4) above determine the spinors $\{v(k_{xn})\}$ used in Eq. (4). A similar procedure applies for the wave vectors $\{q_{xn}(\varepsilon)\}$ and the spinors $w_n(q_{xn})$. They are obtained, respectively, from k_{xn} and $\{v(k_{xn})\}$ after replacing $\varepsilon \to \varepsilon - u_0$.

2. Transmission through a low barrier and partial Klein tunneling

There are various configurations related to Klein transmission through a barrier of height u_0 in the presence of RSOC of strength λ, determined by inequalities involving u_0, ε, and λ. (1) For $0 < u_0 < \varepsilon - 2\lambda < \varepsilon$ [to the left of the blue point in Fig. 7(a) and $1 < T < 2$ in the left of Fig. 7(c)], we have scattering above the barrier with two channels open $q_{x1}^2, q_{x2}^2 > 0$, and there is no tunneling. (2) For $\varepsilon - 2\lambda < u_0 < \varepsilon$ [between the blue and red points in Fig. 7(a), panel 2 in Fig. 7(b), and $0 < T < 1$ in the left of Fig. 7(c)], $q_{x1}^2 > 0$, $q_{x2}^2 < 0$, we have scattering above the barrier with one channel open. This is partial Klein tunneling above the barrier. (3) For $\varepsilon < u_0 < \varepsilon + 2\lambda$ [between the red and green points in Fig. 7(a), panel 4 in Fig. 7(b), and $0 < T < 1$ in the right of Fig. 7(c)], $q_{x1}^2 < 0$, $q_{x2}^2 > 0$, we have scattering below the barrier with one channel open. This is partial Klein tunneling below the barrier. (4) For $0 < \varepsilon + 2\lambda < u_0$ [to the right of the green point in Fig. 7(a), panel 5 in Fig. 7(b), and $1 < T < 2$ in the right of Fig. 7(c)], $q_{x1}^2, q_{x2}^2 > 0$, and we have scattering below the barrier with two channels open. This is full Klein tunneling below the barrier.

3. Spin current densities as function of λ and u_0

Here, we display additional figures showing current densities as a function of barrier height u_0 and RSOC strength λ. Figure 8(a) shows the transmission and the charge current for fixed λ vs u_0 in the region $u_0 > \varepsilon + 2\lambda$, where there is full Klein tunneling. From Eq. (6), it is evident that the pattern of the transmission is that of small oscillations (determined by the trigonometric term in the denominator), just below the maximal value $T = 2$. It is also reasonable to expect that the current is correlated with the transmission (note, however, that the current is space independent, while the transmission is defined only to the right of the barrier). Figures 8(a) and 7(c)
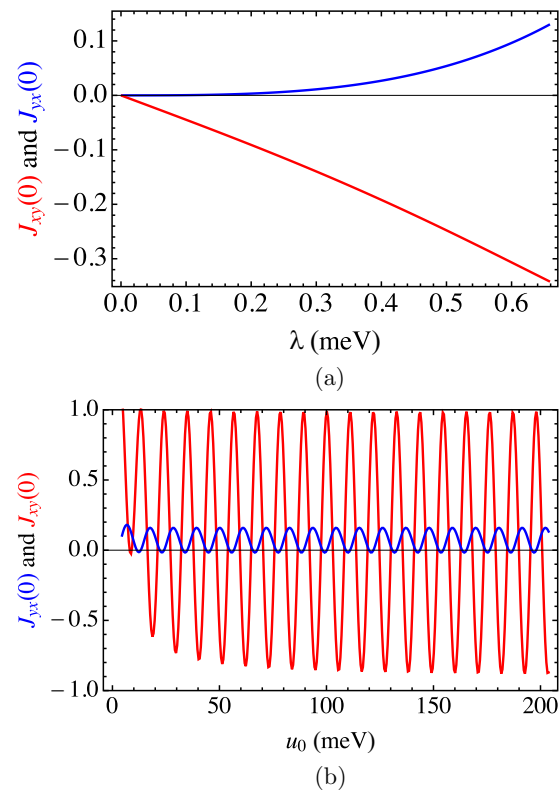

(a)

(b)

FIG. 9. (a) Spin current densities $J_{yx}(0)$ and $J_{xy}(0)$ (in units of J_0) vs λ at the left wall of the barrier ($x = 0$) vs λ for $u_0 = 192$ meV, $d = 200$ nm, and $\varepsilon = 2.60$ meV. Note that the symmetry condition $J_{xy} = -J_{yx}$ valid in bulk SLG is broken by the 1D potential barrier. (b) Spin current densities $J_{xy}(0)$, $J_{yx}(0)$ on the left wall of the barrier vs λ for $\varepsilon + 2\lambda < u_0 < 200$ meV, $d = 200$ nm, $\varepsilon = 2.60$ meV, $\lambda = 0.695$ meV, and $k_y = 0$.

together with Fig. 2 complete our visage of the transmission coefficient as a function of u_0 and λ. Figure 8(b) plots the only nonzero spin density S_y for fixed λ as a function of u_0 in the region $u_0 > \varepsilon + 2\lambda$, where there is full Klein tunneling. Recall that S_y is space independent.

Figure 9(a) shows the spin current densities $J_{xy}(0)$ (red curve) and $J_{yx}(0)$ (blue curve) vs λ, just to the left wall of the barrier for the p-n-p junction. In the main text, these quantities are shown at $x = d$ (that is, the right wall of the barrier). Both $J_{xy}(0)$ and $J_{xy}(d)$ are nearly linear with λ but have different signs. The size of the spin current density $J_{xy}(0)$ (electrons polarized along x and propagated along y) for $\lambda \approx 0.659$ meV is indeed large (same order of magnitude as in J_{xy} calculated in bulk SLG for $\lambda \approx 45$ meV, that is, about two orders of magnitude higher than the value of λ used here). Figure 9(b) shows the spin current densities $J_{xy}(0)$ (red curve) and $J_{yx}(0)$ (blue curve) as a function of λ on the left wall of the barrier. Compare this with Fig. 5, where these quantities are shown at the right wall of the barrier at $x = d$.

4. Space dependence of spin current density, continuity equation, and spin torque

In the general case of a three-dimensional material, the observable spin current density tensor $J_{ij}(\mathbf{r}, t)$ depends on space

and time. For each polarization direction $i = 1, 2, 3 = x, y, z$, the vector field

$$\mathbf{J}_i(\mathbf{r}, t) = [J_{ix}(\mathbf{r}, t), J_{iy}(\mathbf{r}, t), J_{iz}(\mathbf{r}, t)], \quad (A5)$$

satisfies the continuity equation

$$\frac{\partial S_i(\mathbf{r}, t)}{\partial t} + \nabla \cdot \mathbf{J}_i(\mathbf{r}, t) = \mathcal{T}_i(\mathbf{r}, t) \equiv \text{Re}[\psi^\dagger(\mathbf{r}, t)\hat{\mathcal{T}}_i \psi(\mathbf{r}, t)].$$

Here, the scalar $\mathcal{T}_i(\mathbf{r}, t)$ is the spin torque density, and $\hat{\mathcal{T}}_i = \frac{1}{i\hbar}[\hat{S}_i, H]$ is the spin torque density operator, where $H = (\mathbf{p} + \lambda \boldsymbol{\sigma} \times \mathbf{n}_E) \cdot \boldsymbol{\tau}$ is the Hamiltonian operator, and $\mathbf{n}_E$ is the unit vector in the direction of the electric field. The volume integral of $\mathcal{T}_i(\mathbf{r}, t)$ sometimes vanishes due to symmetry relations [58], and then there exists a vector field $\mathbf{P}_i(\mathbf{r}, t)$ such that $\mathcal{T}_i(\mathbf{r}, t) =$

$-\nabla \cdot \mathbf{P}_i(\mathbf{r}, t)$. Because $k_y = 0$, the space dependence varies only with x. Hence, in the static case the continuity equation becomes

$$\mathcal{T}_i(x) = \frac{dJ_i(x)}{dx}. \quad (A6)$$

For 2D systems, with $J_{iz}(x) = 0$, the nonzero two component vector fields are

$$\mathbf{J}_1(x) = [0, J_{xy}(x)], \quad \mathbf{J}_2(x) = [J_{yx}(x), 0]. \quad (A7)$$

According to our discussion above, the only nonzero torque density scalar field is

$$\mathcal{T}_y(x) = \frac{dJ_{yx}(x)}{dx}. \quad (A8)$$

[1] K. S. Novoselov, A. K. Geim, S. V. Morozov, D. Jiang, Y. Zhang, S. V. Dubonos, I. V. Grigorieva, and A. A. Firsov, Science **306**, 666 (2004); A. K. Geim and K. S. Novoselov, Nature Mater. **6**, 183 (2007); A. K. Geim, Science **324**, 1530 (2009).

[2] A. H. Castro Neto, F. Guinea, N. M. R. Peres, K. S. Novoselov, and A. K. Geim, Rev. Mod. Phys. **81**, 109 (2009).

[3] S. Das Sarma, S. Adam, E. H. Hwang, and E. Rossi, Rev. Mod. Phys. **83**, 407 (2011).

[4] O. Klein, Z. Phys. **53**, 157 (1929); C. W. J. Beenakker, Rev. Mod. Phys. **80**, 1337 (2008).

[5] M. I. Katsnelson, K. S. Novoselov, and A. K. Geim, Nat. Phys. **2**, 620 (2006).

[6] T. Tudorovskiy, K J. A. Reijnders and M. I. Katsnelson, Phys. Scr. **T146**, 014010 (2012).

[7] V. V. Cheianov and V. I. Fal'ko, Phys. Rev. B **74**, 041403(R) (2006).

[8] Pierre E. Allain and J.-N. Fuchs, Eur. Phys. J. B **83**, 301 (2011).

[9] T. Ando and T. Nakanishi, J. Phys. Soc. Jpn. **67**, 1704 (1998).

[10] J. M. Pereira, Jr., V. Molnar, F. M. Peeters, and P. Vasilopoulos, Phys. Rev. B **74**, 045424 (2006).

[11] M. Barbier, P. Vasilopoulos, and F. M. Peeters, Phil. Trans. R. Soc. A **368**, 5499 (2010).

[12] Y. Avishai and Y. B. Band, Phys. Rev. B **102**, 085435 (2020).

[13] D. Huertas-Hernando, F. Guinea, and A. Brataas, Phys. Rev. B **74**, 155426 (2006).

[14] H. Min, J. E. Hill, N. A. Shinitsyn, B. R. Sahu, L. Kleinman, and A. H. MacDonald, Phys. Rev. B **74**, 165310 (2006).

[15] Y. Yao, F. Ye, X. L. Qi, S. C. Zhang, and Z. Fang, Phys. Rev. B **75**, 041401(R) (2007).

[16] E. V. Castro, K. S. Novoselov, S. V. Morozov, N. M. R. Peres, J. M. B. L. dos Santos, J. Nilsson, F. Guinea, A. K. Geim, and A. H. Castro Neto, Phys. Rev. Lett. **99**, 216802 (2007).

[17] B. Trauzettel, D. V. Bulaev, D. Loss, and G. Burkard, Nat. Phys. **3**, 192 (2007).

[18] N. Tombros, C. Jozsa, M. Popinciuc, H. T. Jonkman, and B. J. van Wees, Nature (London) **448**, 571 (2007).

[19] N. Tombros, S. Tanabe, A. Veligura, C. Jozsa, M. Popinciuc, H. T. Jonkman, and B. J. van Wees, Phys. Rev. Lett. **101**, 046601 (2008).

[20] S. Cho, Y. Chen, and M. S. Fuhrer, Appl. Phys. Lett. **91**, 123105 (2007).

[21] M. Zarea and N. Sandler, Phys. Rev. B **79**, 165442 (2009).

[22] E. I. Rashba, Phys. Rev. B **79**, 161409(R) (2009).

[23] M.-H. Liu and C.-R. Chang, Phys. Rev. B **80**, 241304(R) (2009).

[24] M. Gmitra, S. Konschuh, C. Ertler, C. Ambrosch-Draxl, and J. Fabian, Phys. Rev. B **80**, 235431 (2009).

[25] D. Bercioux and A. De Martino, Phys. Rev. B **81**, 165410 (2010).

[26] S. Konschuh, M. Gmitra, and J. Fabian, Phys. Rev. B **82**, 245412 (2010).

[27] F. Schwierz, Nature Nanotechnol. **5**, 487 (2010).

[28] W.-K. Tse, Z. Qiao, Y. Yao A. H. MacDonald, and Q. Niu, Phys. Rev. B **83**, 155447 (2011).

[29] S. Konschuh, Spin-orbit coupling effects from graphene to graphite, Ph.D. thesis, Universität Regensburg, 2011.

[30] G. Miao, M. Münzenberg, and J. S. Moodera, Rep. Prog. Phys. **74**, 036501 (2011).

[31] S. Jo, D.-K. Ki, D. Jeong, H.-J. Lee, and S. Kettemann, Phys. Rev. B **84**, 075453 (2011).

[32] J. F. Liu, B. K. S. Chan, and J. Wang, Nanotechnology **23**, 095201 (2012).

[33] D. Marchenko, A. Varykhalov, M. R. Scholz, G. Bihlmayer, E. I. Rashba, A. Rybkin, A. M. Shikin, and O. Rader, Nat. Commun. **3**, 1232 (2012).

[34] M.-H. Liu, J. Bundesmann, and K. Richter, Phys. Rev. B **85**, 085406 (2012).

[35] A. K. Patra, S. Singh, B. Barin, Y. Lee, J.-H. Ahn, E. del Barco, E. R. Mucciolo, and B. Özyilmaz, Appl. Phys. Lett. **101**, 162407 (2012).

[36] B. Dulbak, M. B. Martin, C. Deranlot, B. Servet, S. Xavier, R. Mattana, M. C. Berger, W. A. De Heer, F. Petroff, A. Anane, and P. Seneor, and A. Fert, Nature Phys. **8**, 557 (2012).

[37] P. J. Zomer, M. H. D. Guimarães, N. Tombros, and B. J. van Wees, Phys. Rev. B **86**, 161416(R) (2012).

[38] Q. Zhang, K. S. Chan, Z. Lin, and J. F. Liu, Phys. Lett. A **377**, 632 (2013).

[39] L. Lenz, D. F. Urban, and D. Bercioux, Eur. Phys. J. **86**, 502 (2013).

[40] K. Shakouri, M. R. Masir, A. Jellal, E. B. Choubabi, and F. M. Peeters, Phys. Rev. B **88**, 115408 (2013).

[41] Z. Tang, E. Shikoh, H. Ago, K. Kawahara, Y. Ando, T. Shinjo, and M. Shiraishi, Phys. Rev. B **87**, 140401(R) (2013).

[42] W. Han, R. K. Kawakami, M. Gmitra, and J. Fabian, Nat. Nanotechnol. **9**, 794 (2014).

[43] D. Kochan, M. Gmitra, and J. Fabian, Phys. Rev. Lett. **112**, 116602 (2014).

[44] D. V. Tuan, F. Ortmann, D. Soriano, S. O. Valenzuela, and S. Roche, Nat. Phys. **10**, 857 (2014).

[45] M. Gmitra and J. Fabian, Phys. Rev. B **92**, 155403 (2015).

[46] A. C. Ferrari *et al.*, Nanoscale **7**, 4598 (2015).

[47] S. Roche, J. Åkerman, B. Beschoten, J.-C. Charlier, M. Chshiev, S. Prasad Dash, B. Dlubak, J. Fabian, A. Fert, M. Guimaräes, F. Guinea, I. Grigorieva, C. Schönenberger, P. Seneor, C. Stampfer, S. O. Valenzuela, X. Waintal, and B. van Wees, 2D Materials, **2**, 030202 (2015).

[48] H. Zhang, Z. Ma, and J. F. Liu, Sci. Rep. **4**, 6464 (2014).

[49] M. Drögler, C. Franzen, F. Volmer, T. Pohlmann, L. Banszerus, M. Wolter, K. Watanabe, T. Taniguchi, C. Stampfer, and B. Beschoten, Nano Lett. **16**, 3533 (2016).

[50] A. Avsar, I. J. Vera-Marun, J. Y. Tan, G. K. W. Koon, K. Watanabe, T. Taniguchi, S. Adam, and B. Özyilmaz, NPG Asia Mater. **8**, e274 (2016).

[51] J. Ingla-Aynés, R. J. Meijerink, and B. J. van Wees, Nano Lett. **16**, 4825 (2016).

[52] B. Berche, F. Mireles, and E. Medina, Condens. Matter Phys. **20**, 13702 (2017).

[53] X. Li, Z. Wu, and J. Liu, Sci. Rep. **7**, 6526 (2017).

[54] X. Lin, L. Su, Z. Si, Y. Zhang, A. Bournel, Y. Zhang, J.-O. Klein, A. Fert, and W. Zhao, Phys. Rev. Applied **8**, 034006 (2017).

[55] A. M. Afzal, K. H. Min, B. M. Ko, and J. Eom, RSC Adv. **9**, 31797 (2019).

[56] S. Qi, Y. Han, F. Xu, X. Xu, and Z. Qiao, Phys. Rev. B **99**, 195439 (2019).

[57] E. I. Rashba, Sov. Phys. Solid State **2**, 1109 (1960); Y. A. Bychkov, and E. I. Rashba, JETP Lett. **39**, 78 (1984); H. A. Engel E. I. Rashba, and B. I. Halperin, arXiv:cond-mat/0603306.

[58] J. Shi, P. Zhang, D. Xiao, and Q. Niu, Phys. Rev. Lett. **96**, 076604 (2006).

[59] D. D. Awschalom, D. Loss, and N. Samarth (eds.), *Semiconductor Spintronics and Quantum Computation* (Springer, Berlin, 2002).

[60] I. Zutic, J. Fabian, and S. Das Sarma, Rev. Mod. Phys. **76**, 323 (2004).

[61] N. Hatano, R. Shirasaki, and H. Nakamura, Phys. Rev. A **75**, 032107 (2007).

[62] S. Matityahu, Y. Utsumi, A. Aharony, O. Entin-Wohlman, and C. A. Balseiro, Phys. Rev. B **93**, 075407 (2016).

[63] Y. Avishai and Y. B. Band, Phys. Rev. B **95**, 104429 (2017).